Journal of Power Sources 247 (2014) 294–306

Contents lists available at ScienceDirect

Journal of Power Sources

journal homepage: www.elsevier.com/locate/jpowsour

4E analysis and multi objective optimization of a micro gas turbine and solid oxide fuel cell hybrid combined heat and power system

Sepehr Sanaye*, Arash Katebi

Energy Systems Improvement Laboratory (ESIL), Department of Mechanical Engineering, Iran University of Science and Technology (IUST), Narmak, Tehran 16844, Iran

HIGHLIGHTS

- Energy, exergy, economic and environmental (4E) modeling of SOFC–MGT CHP system.
- Obtaining optimal values of design parameters by defining new objective functions.
- Performing sensitivity analysis with variation of fuel cost and capital investment.

ARTICLE INFO

Article history:
Received 25 June 2013
Received in revised form
4 August 2013
Accepted 16 August 2013
Available online 31 August 2013

Keywords:
Solid oxide fuel cell
Micro gas turbine
CHP system
4E analysis and optimization

ABSTRACT

Energy, exergy, economic and environmental (4E) analysis and optimization of a hybrid solid oxide fuel cell and micro gas turbine (SOFC–MGT) system for use as combined generation of heat and power (CHP) is investigated in this paper. The hybrid system is modeled and performance related results are validated using available data in literature. Then a multi-objective optimization approach based on genetic algorithm is incorporated. Eight system design parameters are selected for the optimization procedure. System exergy efficiency and total cost rate (including capital or investment cost, operational cost and penalty cost of environmental emissions) are the two objectives. The effects of fuel unit cost, capital investment and system power output on optimum design parameters are also investigated. It is observed that the most sensitive and important design parameter in the hybrid system is fuel cell current density which has a significant effect on the balance between system cost and efficiency. The selected design point from the Pareto distribution of optimization results indicates a total system exergy efficiency of 60.7%, with estimated electrical energy cost 0.057 $\$kW^{-1}\ h^{-1}$, and payback period of about 6.3 years for the investment.

1. Introduction

The world's increasing energy demand and the environmental impacts of fossil fuel utilization in conventional power plants have attracted much interest to the development of clean and high efficiency energy systems. Still majorly relying on fossil fuels, fuel cells stand as the most promising technology for their ability to avoid combustion emissions due to the fact that they directly convert the chemical energy of fuel into electricity. High efficiency, clean operation and fuel flexibility of fuel cells has made them a very attractive choice [1] for energy specialists. The solid oxide fuel cell has advantages such as increasing power output and efficiency over other types of fuel cells in power generation industries when they are used as a bottoming cycle with a gas turbine. The resulted hybrid system can reach the first law efficiency levels more than 60% and overall thermal efficiency more than 80% [2]. This system is applicable for small scale plants by coupling with micro gas turbines (MGTs) for distributed generation. Modeling and optimizing the hybrid SOFC–micro gas turbine system is a subject of interest. Lubelli and Massardo [3] performed a comprehensive study on different layouts of hybrid SOFC–GT systems for the atmospheric and pressurized configurations and studied their performance under the effects of different parameters. Campanari [4] and Costamagna [5] predicted the performance of a hybrid MGT–SOFC system in both full load and part load conditions for mode and speed control. Chan et al. [6–10] proposed an accurate model for the electrochemical behavior of the fuel cell and studied the effects of various parameters on the simple and hybrid SOFC systems in full and part loads which provided a means for sizing the system. Massardo and Magistri [11] performed an exergy analysis on the

* Corresponding author. Tel./fax: +98 21 77240192.
E-mail address: sepehr@iust.ac.ir (S. Sanaye).

0378-7753/$ – see front matter © 2013 Elsevier B.V. All rights reserved.
http://dx.doi.org/10.1016/j.jpowsour.2013.08.065

Nomenclature

ACPR	air compressor pressure ratio
A_t	heat transfer area (m^2)
$\dot{C}$	cost rate ($\$s^{-1}$)
C	cost ($)
c	specific cost ($\$kg^{-1}$), ($\$kW^{-1}\ h^{-1}$)
$\overline{C}_p$	specific heat (kJ mol^{-1})
$\dot{E}$	exergy rate (kW)
e	specific exergy (kJ kg^{-1})
F	Faraday's Constant
FCPR	fuel compressor pressure ratio
g_f^0	Gibbs function of formation (kJ kg^{-1})
$\dot{H}$	enthalpy rate (kW)
h	enthalpy (kJ kg^{-1})
h_f^0	enthalpy of formation (kJ kg^{-1})
I	electric current (A)
i	current density, interest rate (Am^{-2}), (%)
K_p	chemical equilibrium constant
LHV	lower heating value (kJ kg^{-1})
LMTD	logarithmic mean temperature difference (K)
$\dot{m}$	mass flow rate (kgs^{-1})
N	number of working hours per year (hours)
n	system lifetime (years)
$\dot{n}$	molar flow rate (kmol s^{-1})
P	pressure (bar)
p	payback period (years)
$\dot{Q}$	heat transfer rate (kW)
R	universal gas constant (kJ $kmol^{-1}\ K^{-1}$)
S/C	steam to carbon ratio
T	temperature (K)
TPR	turbine pressure ratio
U	overall heat transfer coefficient (Wm^{-2} K)
U_f	fuel utilization factor
V	voltage, volume (Volt), (m^3)
$\dot{W}$	power (kW)
x, y, z	chemical reaction rate (kmol s^{-1})

Subscripts

AC	air compressor
AIP	air injection pipe
An	anode
AUX	auxiliary
act	activation voltage loss
c	cold
Ca	cathode
Cap	capital
CC	combustion chamber
Conc	concentration voltage loss
El	electrochemical
env	environmental
ex	exergetic
f	fuel
FC	fuel compressor
FPH	fuel pre-heater
h	hot
HR	heat recovery
O&M	operation and maintenance
Ohm	Ohmic voltage loss
react	reaction
REC	recuperator
Ref	reforming reaction
Rev	reversible
Shift	shifting reaction
T	turbine

Greek symbols

ε	effectiveness
η	efficiency, voltage loss
φ	maintenance factor

hybrid system and carried out a thermo-economic study on this system by proposing cost models. Bavarsad [12] investigated the hybrid system from the second law viewpoint as well as effects of various parameters on the exergy destruction in system components. Calise et al. [13–16] modeled and analyzed the hybrid system from energy, exergy and economic aspects and performed a single level thermo-economic optimization analysis. Autissier et al. [17] used an optimization approach to design the hybrid system for two objectives of efficiency and cost. Duan et al. [18] performed a parametric optimization of the hybrid SOFC-MGT system.

However, in the most of above research works the first law efficiency was applied as the criteria for evaluating the system performance, this paper proposes four E (energy, exergy, economic, environmental) analysis and multi-objective optimization for estimating the values of interested design parameters (decision variables) of a hybrid SOFC and micro gas turbine CHP system. Two objective functions used in optimization procedure were the exergy efficiency and system total cost rate. The environmental penalty cost caused by CO_2 emissions was also added to the total cost. An optimization procedure based on genetic algorithm has been incorporated to reach the optimum design parameters with regard to a set of constraints. The results were discussed and an optimum solution point was selected from the Pareto front. The exergy destruction in system components and effects of optimization on the exergy destruction has been studied, in a next step the sensitivity analysis of the optimum solutions to different parameters were performed. The followings are the contribution of this paper into the subject:

- Simultaneous energy, exergy, economic and environmental (4E) modeling and analysis of the hybrid SOFC–MGT CHP system was performed to predict the system performance, for generating combined heat and power.
- The optimal values of system design parameters were estimated using new objective functions, new design parameters and a list of constraints.
- Performing sensitivity analysis of the system to study the change in optimum values of design parameters with variation of fuel cost as well as the capital investment and system power output.

2. Plant description

The SOFC–MGT system layout is depicted in Fig. 1. This configuration includes all critical thermal processes of a direct coupled internal reforming SOFC–MGT hybrid system in a simplified manner and is close to the first real constructed system of its kind [2,4].

The system consists of the following processes:

Air (point 1) and CH_4 fuel (point 9) at known inlet conditions pass through compressors (AC and FC). These streams (points 2 and

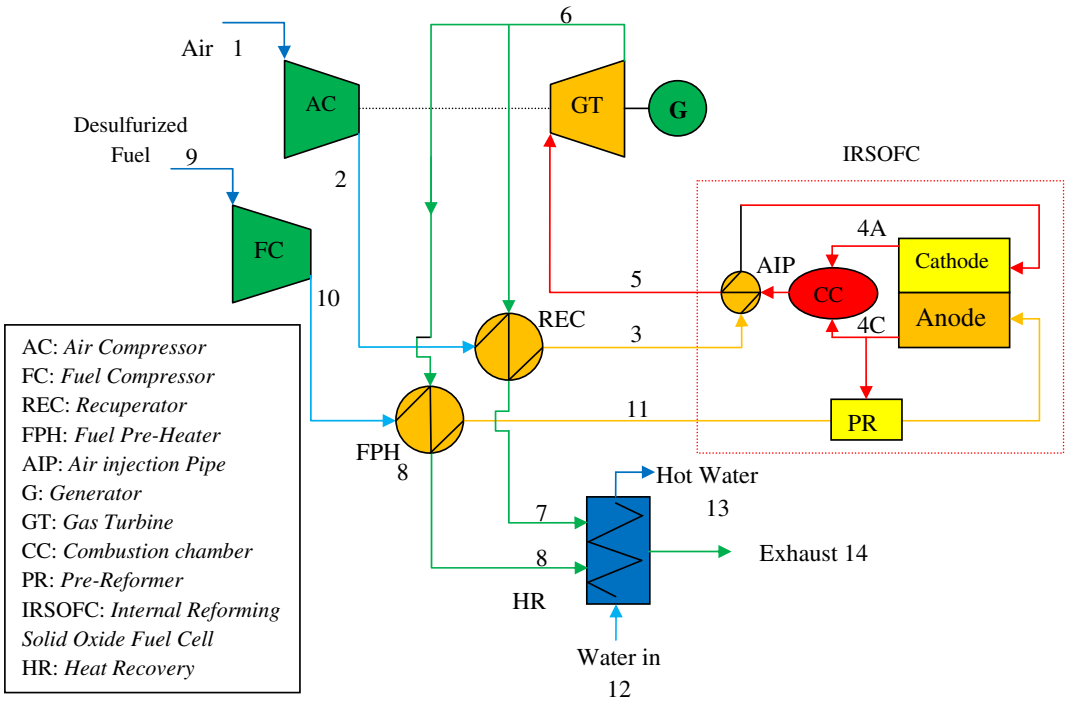

Fig. 1. Plant layout.

10) are preheated in recuperator (REC) and fuel preheater (FPH) respectively using the recovered energy from turbine exhaust gases. Since only hydrogen can participate in the electrochemical reaction of the fuel cells, natural gas should be reformed to hydrogen rich products in presence of steam at high temperature and pressures. By design, the internal structure of SOFC allows for a large portion of fuel conversion to take place at the pressure and temperature of the fuel cell itself by means of internal reforming capability. The heat needed to drive the reforming process can be produced by exothermic electrochemical reaction. It is also vital in direct reforming that some percentage of inlet methane be converted to hydrogen before entering the anode compartment in a pre-reforming reactor. The steam needed for these reactions can be provided by recirculation of the anode outlet products to the entering stream. By this way the need to a costly separate steam generator would be eliminated. On the other side, air after recuperation (at point 3) passes through another pre-heater (Air injection pipe, AIP) and then is sent to the cathode. Then the electrochemical reaction takes place on the three phase boundaries of the electrodes where a large amount of electrical and thermal energy is released. In this type of fuel cells, the air before reaching the electrode surface is heated again in the air injection pipes by the heat of combustion reaction. This occurs when the outlet streams from the anode and excess air from the cathode get mixed (Fig. 2) where not reacted fuel and all combustible products are fully oxidized. For this reason the air injection pipes are modeled by use of a virtual heat exchanger. Hot gases after this point (5) are expanded trough a radial gas turbine where additional power is extracted. The combustion products which one produced in the combustion compartment (CC) and passed through the turbine are mainly sent to the recuperator (about 95% in stream 7) while the rest about 5 percents is sent to fuel pre-heater (stream 8). The exhaust flow (stream 14) still has sufficient thermal energy to be recovered for domestic water heating consumptions in a heat recovery exchanger (HR). The desulfurized inlet fuel permits the system exhaust gases to be cooled down to as low as 50 °C without the risk of formation of sulfuric acid and stack corrosion [2].

3. Thermal modeling

For thermal modeling of the system in steady state condition the average values of the thermodynamic parameters at each component were applied. In this model the gradients of temperature and pressure in the fuel cell as well as other components were neglected and the equilibrium outlet temperature of fuel cell stack was considered as its working temperature. For thermophysical properties of gases, a temperature dependent specific heat model based on empirical polynomials for ideal gas was applied.

3.1. Compressors and gas turbine

The outlet temperatures of fuel and air compressors as well as the gas turbine were computed from the following equations by try and error scheme.

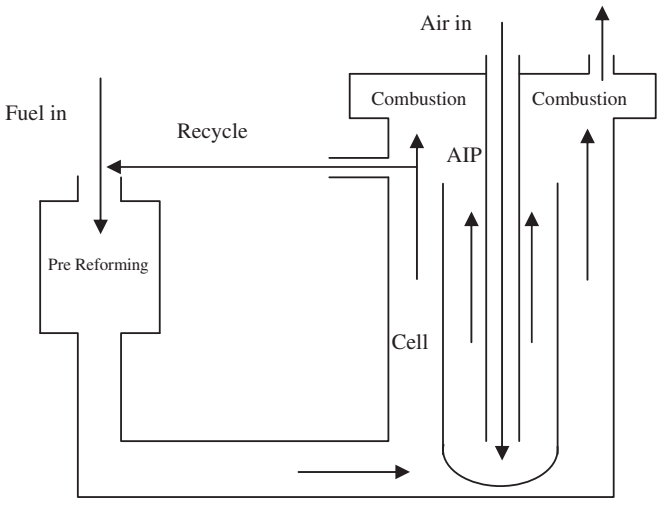

Fig. 2. Internal reforming tubular SOFC schematic.

For air and fuel compressors:

$$\int_{T_1}^{T_2} \overline{C}_{p,\mathrm{air}} \frac{\mathrm{d}T}{T} = \frac{R}{\eta_{\mathrm{AC}}} \ln(\mathrm{ACPR}) \tag{1}$$

$$\int_{T_9}^{T_{10}} \overline{C}_{p,\mathrm{fuel}} \frac{\mathrm{d}T}{T} = \frac{R}{\eta_{\mathrm{FC}}} \ln(\mathrm{FCPR}) \tag{2}$$

For turbine:

$$\int_{T_5}^{T_6} \overline{C}_{p,\mathrm{gas}} \frac{\mathrm{d}T}{T} = R\eta_T \ln(\mathrm{TPR}) \tag{3}$$

$$\overline{C}_{p,\mathrm{gas,avg}} \ln\left(\frac{T_6}{T_5}\right) = R\eta_T \ln(\mathrm{TPR}) \tag{4}$$

3.2. Heat exchangers

The design specifications of recuperator and fuel pre-heater (plate fin type heat exchanger) were obtained by using ε-NTU method for cross flow configuration without mixing of hot and cold fluids [19]. For known design effectiveness, the unknown temperatures could be computed from the following equations in which the specific heat values were estimated at the hot (h) or cold (c) side temperatures.

$$\varepsilon = \frac{C_h(T_{h1} - T_{h2})}{C_{\min}(T_{h1} - T_{c1})} \text{ or } \frac{C_c(T_{c2} - T_{c2})}{C_{\min}(T_{h1} - T_{c1})} \tag{5}$$

The heat transfer surface area for each exchanger was then obtained from the definition of number of transfer units (NTU) and its relation with effectiveness (ε). Appropriate equations and data in Refs. [20–24] were used to compute the overall heat transfer coefficient.

The air injection pipes were also modeled as a cross flow heat exchanger and were assumed to be an integrated part of the stack. Furthermore a shell and tube type heat exchanger was selected for heat recovery, for which the following relations were used to determine the heat transfer surface area:

$$A_t = \frac{\dot{Q}}{U\Delta T_{\mathrm{mean}}} \tag{6}$$

$$\Delta T_m = 0.9\Delta T_{\mathrm{LMTD}} \tag{7}$$

The average value of overall heat transfer coefficient was considered to be 100 $\mathrm{Wm^{-2}\,K^{-1}}$ [23].

3.3. SOFC internal reforming

The solid oxide fuel cell was based on a tubular, internal reforming design, for which the performance related data and design parameters were taken from [6,13,15]. The fuel cell modeling was performed in three steps. At the first step, all internal chemical reactions and their rates were determined by the chemical equilibrium model by which the kinetic conditions and molar flow rates of species were found. The output cell voltage and electrical power was then computed by means of an electrochemical model considering all major voltage losses in the cell based on its working parameters. Finally, a conventional first law energy balance was used to determine the temperature and thermodynamic state of exiting flows from the stack.

3.3.1. Chemical equilibrium model

It is assumed that the following reactions take place inside the stack and each individual cell. From which at the anode compartment, the reforming and shifting reactions were supposed to be in chemical equilibrium. In order to determine the composition of outlet gases from the cell, the following reactions were studied:

$$x\mathrm{CH_4} + x\mathrm{H_2O} \leftrightarrow x\mathrm{CO} + 3x\mathrm{H_2}\ \text{Reforming} \tag{8.1}$$

$$y\mathrm{CO} + y\mathrm{H_2O} \leftrightarrow y\mathrm{CO_2} + y\mathrm{H_2}\ \text{Shifting} \tag{8.2}$$

$$z\mathrm{H_2} + z\left(\frac{1}{2}\mathrm{O_2}\right) \leftrightarrow z\mathrm{H_2O}\ \text{Electrochemical} \tag{8.3}$$

where: x, y and z, denote the rate of reforming, shifting and overall electrochemical reactions respectively.

The constants of equilibrium for each reaction can be described in terms of partial pressures of reactants and products or concentration of these species as follows:

$$K_{P,R} = \frac{P_{\mathrm{CO}} P_{\mathrm{H_2}}^3}{P_{\mathrm{CH_4}} P_{\mathrm{H_2O}}},\ K_{\mathrm{P,S}} = \frac{P_{\mathrm{CO_2}} P_{\mathrm{H_2}}}{P_{\mathrm{CO}} P_{\mathrm{H_2O}}} \tag{9}$$

The values of equilibrium constants can also be obtained from the experimental data in terms of temperature dependent polynomials as follows, for which the constants can be found in Ref. [7].

$$\log(K_P) = AT^4 + BT^3 + CT^2 + DT + E \tag{10}$$

Due to the high rate of reforming reaction in the forward direction and the significant value of its equilibrium constant, this reaction can be assumed to be driven to completion. This assumption avoids the formation of a highly nonlinear system of equations [13].

Having known the rate values and establishing the equilibrium relations in terms of molar concentrations taken form kinetics of each reaction and by knowing that the molar rate of hydrogen participated at the electrochemical reaction was controlled by the fuel utilization factor (which is a design parameter), a system of three equations with three unknowns (x, y, z) was formed as the following:

$$x = \dot{n}_{\mathrm{CH_4,in}} \tag{11.1}$$

$$K_{P,S} = \frac{(\dot{n}_{\mathrm{H_2,in}} + 3x + y - z)(\dot{n}_{\mathrm{CO_2,in}} + y)}{(\dot{n}_{\mathrm{H_2O,in}} - x - y + z)(\dot{n}_{\mathrm{CO,in}} + x - y)} \tag{11.2}$$

$$z = U_f(3x + y) \tag{11.3}$$

By solving this system of equations, the molar composition of exiting flows was determined. Moreover, by the known rate of electrochemical reaction, we could estimate the produced electrical current of the stack. Where F denotes the Faraday's constant.

$$I = 2Fz \tag{12}$$

3.3.2. Electrochemical model

The ideal reversible voltage of the cell can be computed from the Nernst Eq. (13) at its working temperature and pressure of reactants. Where $\Delta\overline{g}_f^0$ denotes the change of Gibbs function for the electrochemical reaction at standard thermodynamic conditions.

$$V_{rev} = -\frac{\Delta\overline{g}_f^0}{2F} + \frac{RT}{2F}\ln\frac{P_{H_2}P_{O_2}^{\frac{1}{2}}}{P_{H_2O}} \quad (13)$$

The actual output voltage was then found by subtracting the voltage drops due to ohmic losses, activation over potential and concentration loss from the ideal cell voltage as follows:

$$V = V_{rev} - \eta_{ohm} - (\eta_{act,An} + \eta_{act,Ca}) - \eta_{Conc} \quad (14)$$

These losses are calculated based on cell working parameters and its design specifications using the relations and data in Ref. [6].

3.3.3. The energy balance

The first law of thermodynamics and energy balance for the whole stack was established as follows for the enthalpy rate of input and output streams, the electrical power produced and the total heat rate released due to internal reactions:

$$\dot{H}_{in} + \dot{H}_{react} = \dot{W} + \dot{H}_{out} \quad (15.1)$$

$$\dot{H}_{react} = -\left(z\Delta h_{el} + y\Delta h_{Shift} + x\Delta h_{Ref}\right) \quad (15.2)$$

$$\dot{H}_{in} = \sum \dot{n}_{j,in}\int_{T_o}^{T_{j,in}} \overline{C}_{p,j}\mathrm{d}T \quad (15.3)$$

$$\dot{H}_{out} = \sum \dot{n}_{j,out}\int_{T_o}^{T_{j,out}} \overline{C}_{p,j}\mathrm{d}T \quad (15.4)$$

$$\dot{W} = VI \quad (15.5)$$

3.4. Combustion compartment

It is assumed that the following reactions take place in cells after mixing exiting gases from the anode and exiting excess air from the cathode. By these reactions, it was assumed that all the combustible products exiting the cell anode are oxidized completely. The molar composition of combustion products was defined easily through the reaction kinetics. To find the gas mixture temperature, an energy balance for adiabatic combustion chamber was established in which η_c shows the combustion efficiency.

$$CH_4 + 2O_2 + CO_2 + 2H_2O \quad (16.1)$$

$$CO + \frac{1}{2}O_2 \rightarrow CO_2 \quad (16.2)$$

$$H_2 + \frac{1}{2}O_2 \rightarrow H_2O \quad (16.3)$$

$$\sum_r \dot{n}_j\left(\overline{h}_{f,j}^0 + \int_{T_o}^{T_{in}} \overline{C}_{p,j}\mathrm{d}T\right) \times \eta_c = \sum_p \dot{n}_j\left(\overline{h}_{f,j}^0 + \int_{T_o}^{T_{out}} \overline{C}_{p,j}\mathrm{d}T\right) \quad (16.4)$$

3.5. Modeling algorithm

For the known design parameters, all the above mentioned relations were applied for the thermodynamic modeling of the system. In this study, the whole model was developed as a computer code in MATLAB software. Since there was a high integrity and interdependency between the system components, direct calculation of many parameters was not possible at the first step. Some parameters such as inlet temperature of gases into the heat exchangers were not known at this stage and they were estimated through a try and error procedure. As the main strategy of modeling algorithm, a guessed value was assigned to the SOFC working temperature (T_4). Based on this temperature and other known design parameters, as well as an estimated value for pressure losses, the constants of equilibrium in Eq. (10) for reactions in SOFC modeling were determined. Then with the known assumed inlet flow rates of air and fuel, the system of Eq. (9) was solved to find the rates of internal reactions (Eq. (8)). Based on these known rates, the exiting gases molar compositions were estimated from the kinetics relations (Eq. (8)). Then the combustion relations (Eq. (16)) were applied and the molar composition and temperature of turbine inlet stream were determined. These data provided all system flow temperature values. In order to evaluate the guessed SOFC working temperature (T_4) value, the energy balance equation (Eq. (15)) was applied. Then the SOFC outlet temperature (T_4) was modified by the energy balance relations until reaching a convergence value for the SOFC temperature (T_4). The flowchart in Fig. 3 shows the whole process of system thermal modeling. Due to need for large number of iterations in computation, the system modeling was very time consuming. Therefore the modified weight coefficients were applied to accelerate the program convergence.

4. Exergy analysis

The rate of exergy was found in all flow lines of the system from known thermodynamic states and molar compositions by relative chemical and physical equations. The rate of exergy destruction in a component was then computed from the respective exergy balance equations.

$$\sum \dot{E}_{in} = \dot{E}_d + \sum \dot{E}_{out} + \dot{W}_{out} \quad (17)$$

Or in terms of fuel and product exergy streams and definition of exergy efficiency, we get

$$\dot{E}_{fuel} = \dot{E}_{product} + \dot{E}_{destructed} \quad (18)$$

$$\eta_{ex} = \frac{\dot{E}_{product}}{\dot{E}_{fuel}} \quad (19)$$

The relations for fuel and product exergy values are listed in Table 1 for all system components.

5. Economic analysis

Both thermodynamic and economic aspects are important in analysis and optimization of energy systems. Several methods were proposed for the thermo-economic assessment of energy systems. However, the first and second law of thermodynamics in conjunction with economic factors provided us a very powerful tool for the optimization of energy systems. The system total cost in this paper is one of objective functions which should be minimized. The total cost included capital and maintenance expenses, the system operating cost (fuel cost), as well as the environment related costs as described in Section 5.1. The investment cost functions are listed in Table 2 [15,21] for major components in terms of their design parameters. In order to convert these costs into cost rates per unit time, the following relations were used [27].

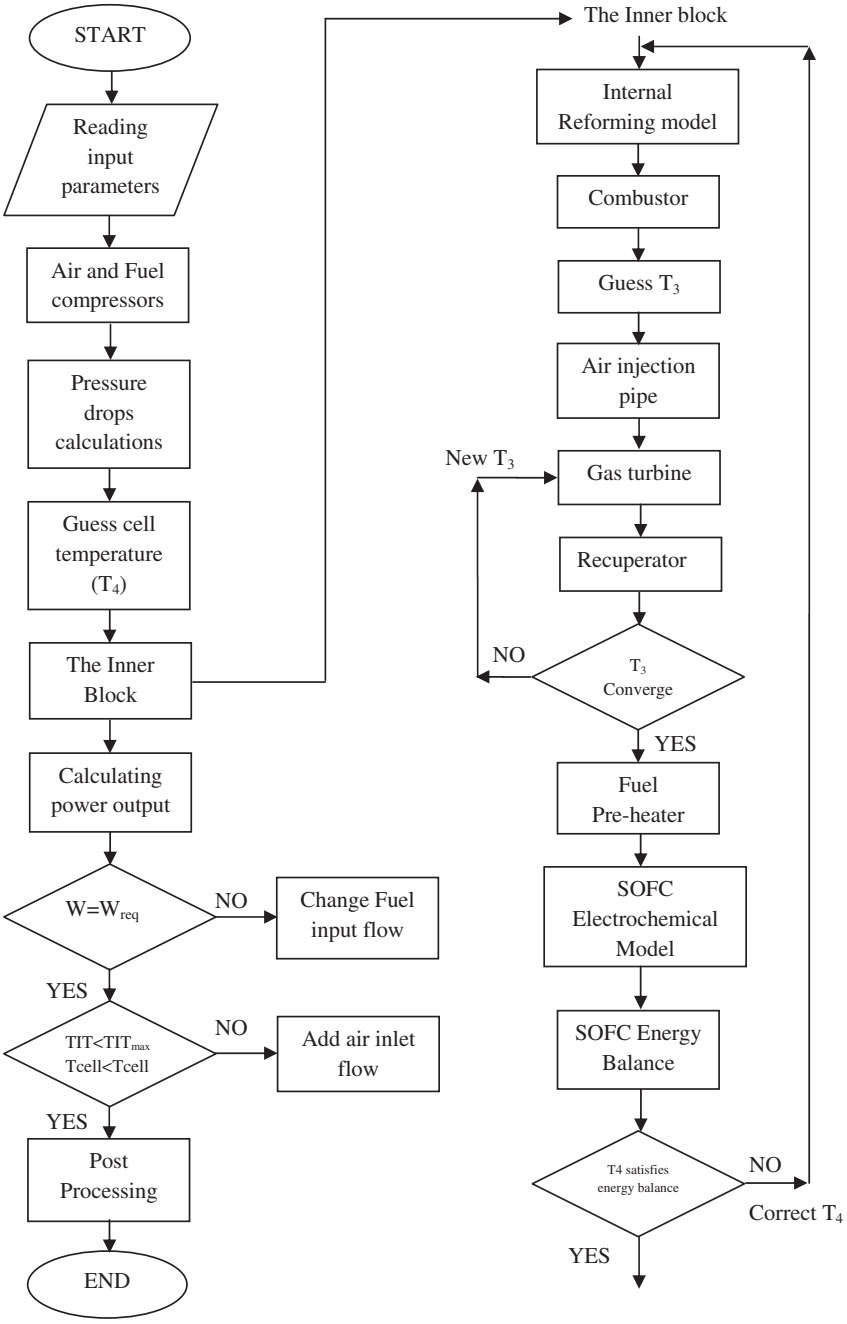

Fig. 3. System thermal modeling flowchart.

Table 1
Exergy relations for the SOFC–MGT system components.

Component	$\dot{E}_{product}$	$\dot{E}_{fuel}$
AC	$\dot{E}_2 - \dot{E}_1$	W_{AC}
FC	$\dot{E}_{10} - \dot{E}_9$	W_{FC}
REC	$\dot{E}_3 - \dot{E}_2$	$\dot{E}_{6,1} - \dot{E}_7$
FPH	$\dot{E}_{11} - \dot{E}_{10}$	$\dot{E}_{6,2} - \dot{E}_8$
SOFC	W_{SOFC}	$(\dot{E}_3 - \dot{E}_{11}) + (\dot{E}_{4A} - \dot{E}_{4C})$
CC	$\dot{E}_{5,1}$	$\dot{E}_{4A} - \dot{E}_{4C}$
AIP	$\dot{E}_{5,2} - \dot{E}_{5,1}$	$\dot{E}_{3,1} - \dot{E}_{3,2}$
GT	W_{GT}	$\dot{E}_5 - \dot{E}_6$
HR	$\dot{E}_{13} - \dot{E}_{12}$	$\dot{E}_7 + \dot{E}_8 - \dot{E}_{14}$

$$\dot{C}_K = \frac{C_K \times \mathrm{CRF} \times \varphi}{N \times 3600} \tag{20.1}$$

$$\mathrm{CRF} = \frac{i(1+i)^n}{(1+i)^n - 1} \tag{20.2}$$

In the above relations C_K shows the capital cost of K^{th} component, CRF is the Capital Recovery Factor which is a function of system lifetime (n) and the annual interest rate (i). φ shows the maintenance factor and N is the total working hours of the system per year. The benefit rate gained by using the heat recovery heat

Table 2
Cost functions for the major components of the SOFC–MGT system.

Component	Cost function ($)
Compressor (centrifugal)	$C_c = 91562(P_c/445)^{0.67}$
Gas turbine (radial)	$C_{GT} = (-98.328\ln(P_{GT}) + 1318.5)P_{GT}$
Recuperator	$C_{REC} = 111.6(m_{HE})^{0.95}$
SOFC stack	$C_{SOFC} = (A_{tot,stack})(2.96T_{cell} - 1907)$
Inverter	$C_{Inv} = 100000(P_{cell}/500)^{0.7}$
Generator	$C_{Gen} = 60(P_{GT} - P_c)^{0.95}$
Auxiliary equipment	$C_{AUx} = 0.1C_{SOFC}$
Heat recovery exchanger	$C_{Ex} = 8500 + 405A_t^{0.85}$

exchanger is expressed in Eq. (21) in terms of difference between the cost of heat recovery heat exchanger and the cost to provide the same required heat by a separate boiler which includes investment cost, operational (fuel) and maintenance costs of the required external boiler.

$$\dot{C}_{Benefit} = \dot{C}_{Ext,Boiler} - \dot{C}_{HR,exchanger} \tag{21}$$

$$\dot{C}_{Ext,Boiler} = \dot{C}_{Cap,Boiler} + \dot{C}_{fuel} + \dot{C}_{O\&M} \tag{22}$$

The Payback period is defined as the time period required for the net income received from selling the output of a system (i.e. Electricity and recovered heat) to recover the initial investment costs of the respective system [27]. Regarding the time value of money, the worth of hybrid system capital investment as well as the fuel consumption costs in the pth year of running can be estimated from the following equation:

$$C_{Invested,p} = \sum_{m=0}^{p-1} C_{cap,m} \times (1+i)^{p-m} + \sum_{m=1}^{p} \dot{C}_{fuel} \times N \times 3600 \times (1+i)^{p-m} \tag{23}$$

where i is the annual interest rate and N is the number of running hours per year.

In a similar way, the net income from selling the output electricity and benefit gained by the heat recovery in the pth year can be calculated as follows:

$$C_{Income,p} = \sum_{m=1}^{p} \left(\dot{W}_{net} \times N \times c_{elec} + \dot{C}_{Benefit} \times N\right)(1+i)^{p-m} \tag{24}$$

According to the definition, the payback period (p) is when these two values in Eqs. (23) and (24) equate. Then p can be computed using an iterative trial and error method.

6. Environmental analysis

Environmental impact is one of the major concerns in analysis of energy systems which is covered in the present study through the optimization of the hybrid SOFC–MGT system. As a general principle, an increase in thermal efficiency of a plant (which provides a specific power output), lowers fuel consumption and decreases emission products such as CO_2. Fuel cells are definitely in a superior situation over the conventional power plants in terms of higher efficiency and lower emissions. Experiments show that the NO_x emissions from a SOFC–MGT system (without any external fuel injection to the combustor) can be less than 1 ppmv [28]. In such systems, the entering fuel must have the lowest sulfur content due to sensitivity of fuel cell parts. Sweetening the inlet fuel prevents the formation of sulfuric acid and other similar pollutants in exhaust gases. In this paper, a penalty cost was associated to the rate of CO_2 emission produced which was added to the system total cost during optimization procedure.

7. Optimization

7.1. Objective functions

In order to find the optimum set of design parameters that provide a trade-off between the cost and performance of hybrid SOFC–MGT system with minimized environmental impacts, a multi objective optimization problem was defined. The first objective function to be maximized was the total exergy efficiency of the system.

$$\text{Obj.Func.I} = \eta_{ex,plant} = \frac{\dot{W}_{net,out}}{\dot{m}_{CH_4,in} e_{CH_4}} \tag{25}$$

The second objective function to be minimized simultaneously was the total cost of the system. This objective function included the capital, operation (fuel) and maintenance costs as well as the environmental penalty costs as follows:

$$\text{Obj.Func.II} = \sum \dot{C}_{Cap,O\&M} + \dot{C}_f + \dot{C}_{env} \tag{26}$$

As the rate of CO_2 production is inversely proportional to the system efficiency (the first objective function), the addition of the latest term in Eq. (26) increases the weight of thermal objective function over the economic objective one as the optimum system tends to be a more efficient system.

Table 3
Optimization constraints and range of variation of design parameters.

Constraint	Description	Range of variation of design parameters	
		From	To
$T(5) < 1203$ K	Turbine inlet temperature limit	–	1203
$T_{cell} < 1500$ K	The maximum temperature value in fuel cell	–	1500
ACPR < 5	The maximum value of single stage compressor pressure ratio	3	5
$S/C > 1.8$	The minimum value for the steam to carbon ratio	1.8	3
$\eta_{AC,T}$<0.85	The maximum isentropic efficiency for the compressor and turbine	0.7	0.85
$0.3 < m_{air,in}$ (kg s^{-1}) < 0.6	Range of values for Air inlet mass flow	0.3	0.6
i (A m^{-2}) < 4000	The maximum value of cell current density	1000	4000
$\varepsilon_{Rec} < 0.9\varepsilon$	The maximum recuperator effectiveness value	0.7	0.9
$U_f < 0.9$	The maximum value of fuel utilization factor	0.7	0.9
$T_{14} > 350$ K	The minimum exhaust gas temperature	350	–

Table 4
Genetic algorithm optimization tuning parameters.

Parameter	Value
Population	120
Maximum number of generations	100
Probability of crossover (P_c)	0.8
Probability of mutation (P_m)	0.01
Selection process	Tournament

7.2. Decision parameters and constraints

The design parameters (decision variables) considered in this optimization problem are the air compressor pressure ratio, the air compressor isentropic efficiency, the gas turbine isentropic efficiency, the inlet air mass flow rate, the cells fuel utilization factor, the cells current density, recuperator effectiveness and the steam to carbon ratio in reformer. To limit the results to a range of feasible points both technically and economically, a set of constraints (Table 3) were applied to the range of decision parameters. The assumed range of change for design parameters is also shown in Table 3.

7.3. Optimization algorithm

The above mentioned optimization is a multi-objective problem that due to its high complexity and nonlinearity and high number of decision parameters, the use of evolutionary algorithms seems to be the best choice as a method of optimization. The evolutionary genetic algorithms (GA) are sort of semi stochastic search methods that imitate the laws of natural evolution for finding an optimal solution to a given problem. This method works in the way that after formation of an initial population of solutions as individuals as different sets of design parameters, pairs of these individuals are selected randomly and they compete in terms of superior gens to form next generations that fulfill the survival of fittest in the nature. With repetition of this procedure for a number of consecutive generations, the results approach to the optimum solution for the system [15]. The multi objective GA in MATLAB optimization toolbox has been implemented in the present study. The parameters for use with the genetic algorithm are listed in Table 4 where the stopping criterion for the algorithm has been set to a specified number of generations.

8. Case study

The hybrid SOFC–MGT system shown in Fig. 1 with 260 kW power and 100 kW heat output (as 80 °C hot water) in full load operation was our case study for the system optimization in the present paper. This configuration is similar to the pressurized hybrid system pioneered by Siemens-Westinghouse in 2000 [28]. For the economic modeling $\varphi = 1.08$ and $N = 8000$ h, the interest rate I = 14% and the unit cost of electricity $c_{elec} = 0.06$ \$kW^{-1} h^{-1} were selected for use in Eqs. (20)–(24) [25,26].

Since the issue of short SOFC lifetime and power degradation affects the economic feasibility of this system. Both the SOFC cost and lifetime estimations were made with future predictions [15]. In this regard, 40000 h lifetime and 0.5% voltage degradation per 1000 h of operation was considered for the SOFC stack [30]. The whole system lifetime (n) was considered equal to 20 years while the SOFC stack is replaced every five years with a salvage value of 1/3 of the purchased equipment [31], while about 20% larger SOFC surface area was assumed to compensate for its voltage degradation during the working time.

Table 5
Verification of modeling Results.

Parameter	Modeling output	Reference [4]	Difference (%)
Cell voltage (V)	0.697	0.7	0.4
SOFC temperature (°C)	994.8	990	0.5
Turbine inlet temperature (°C)	896.7	900	0.3
Micro-turbine power output (kW)	53.2	53.5	0.5
SOFC power output (kW)	218.5	209	4.5
Thermal efficiency (%)	61.8	64.9	5

The fuel cost rate was computed based on unit cost of natural gas (0.13 \$m^{-3} or 0.004 \$MJ^{-1}) and the environmental penalty cost was determined based on the following relation:

$$\dot{C}_{env} = C_{CO_2}\dot{m}_{CO_2} \tag{27}$$

where for C_{CO2} the penalty cost (0.0024 \$)/(kgCO_2) was considered [29].

9. Results and discussion

9.1. Model verification

In order to validate the modeling output results, the operating parameters were compared with the corresponding data reported in Ref. [4] for the same input parameters. Table 5 compares two above groups of data and their corresponding differences in percentage. Results show that the model was capable of predicting the thermal performance of the system quite precisely.

9.2. Optimization results

9.2.1. Pareto front

Two objective functions were defined for the optimization procedure. Maximizing the total exergy efficiency and minimizing the total cost are obviously in conflict with each other and there is distribution of optimal points named Pareto front as depicted in Fig. 4. All single points on Pareto optimal front are optimum non dominated solutions. The point at the farthest RHS shows the highest efficiency as well as the highest total cost. This point has been labeled Point A in Fig. 4 with 62.5% exergy efficiency and

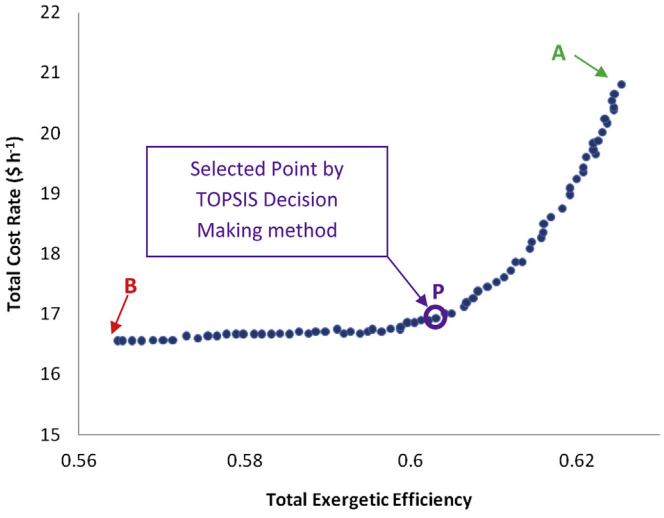

Fig. 4. Pareto front for optimization results.

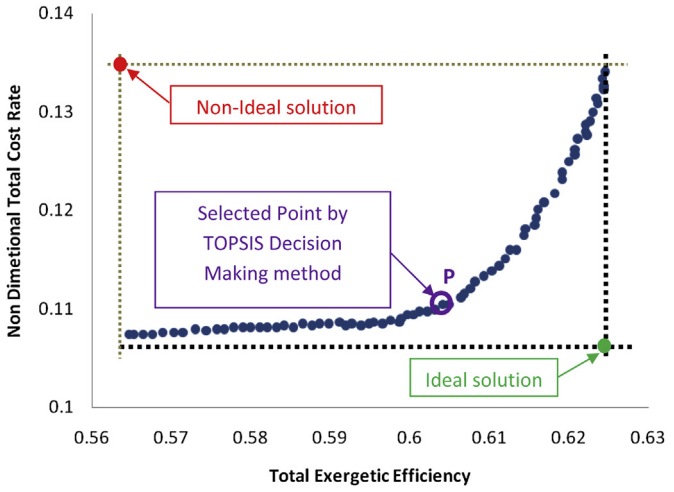

Fig. 5. Non-dimensional Pareto front for optimum point selection using TOPSIS decision making method.

20.71 $\$h^{-1}$ cost rate. The point at the farthest LHS shows the lowest exergy efficiency as well as the lowest total cost. This point has been labeled Point B in Fig. 4 with 56.4% exergy efficiency and 16.44 $\$h^{-1}$ cost rate. Points A and B designate a single objective optimization with only maximum exergy efficiency or minimum Cost in mind respectively. From the behavior of the Pareto front as can be seen in Fig. 4 although the exergy efficiency is increasing from 56.5% to about 60%, the total cost rate only increases slightly. Obviously less fuel consumption and emitted pollution costs weighs out the associated increase in capital cost of the system in this solution points. More rise in the exergy efficiency from 60% to higher values leads to a drastic increment in the total cost rate.

9.2.2. Optimum point selection

In order to choose the best applicable solution on the Pareto front both axes should be non-dimensional making it possible to choose the most optimum point based on the distribution of points and distances from A and B extremes on two sides. To achieve this goal, the Euclidian method has been employed for non-dimensionalizing the total cost rate [32]. The Pareto front distribution of optimal points in non-dimensional form has been plotted in Fig. 5. There are various decision making methods for selecting an optimum point from the points on the non-dimensional Pareto distribution, in this work, the TOPSIS method has been used to select the best optimum solution point [33]. In this method an ideal solution is the imaginary point where each objective has its optimum value regardless of the other objective. On the other hand, a non-ideal solution is the point at which both objectives have their worst values. The two ideal and non-ideal solutions are shown on Fig. 5. The best optimum solution is then selected as the point form the Pareto front which has the shortest distance to the ideal and the longest distance from the non-ideal solution points. The selection is made for the point with minimum closeness coefficient ($d^-/(d^- + d^+)$). Where d^- and d^+ stand for the distances from the ideal and non-ideal points on the non-dimensional Pareto front respectively [33]. Following this method, the point Labeled P in Figs. 4 and 5 has been selected as the final optimum solution. Which corresponds to an exergy efficiency of 60.7% as well as the total cost rate of 16.95 $\$h^{-1}$ with 1.95 $\$h^{-1}$ added for the environmental emission externalized social penalty cost. The payback period estimation is equal to about 6.3 years and the output electrical energy cost (capital and operational investment) is equal to 0.057 $\$kW^{-1}\ h^{-1}$.

9.2.3. Effective design parameters

The variation of design parameters for the range of solutions presented by the Pareto front is shown in Fig. 6a–h. From this figure it can be deduced that the cell current density is the most widely distributed parameter over its allowable domain. This parameter also shows smooth changes versus to the objective functions. This implies that the current density is an effective parameter in balance between the objective functions. It should be noted that the current density is the parameter that determines the cell surface area as well as the SOFC stack cost. Furthermore due to the fact that the exergy destruction of the stack (as the main part of total exergy destruction) was proportional to its current density, therefore the exergy efficiency of the system was also dependent on the cell current density.

The system pressure ratio and air inlet mass flow are the next varying parameters with distributed values over its acceptable domain values. Other parameters are relatively concentrated in constant optimum values and shows that they do not have much effect on the conflict between the objective functions.

The values of design parameters for the optimized case study are listed in Table 6. In Table 7 the dependent parameters of the optimized system are shown which was selected from the Pareto front. In addition, the temperature, pressure and mass flow rates of all system points designated in Fig. 1 are listed in Table 8 for the optimized system. It is noteworthy that the specified steam to carbon ratio in Table 6 requires 53% of the fuel mass flow to be recycled at the SOFC anode as shown in Fig. 2.

9.2.4. Exergy destruction

The values of exergy destruction in the system components are listed in Table 9 for the optimized system. This table shows that the main sources of exergy destruction in the system are the SOFC, combustion chamber and the air injection pipes. This is due to the fact that the major portion of energy conversion takes place in the fuel cells. Furthermore due to high irreversible nature of combustion reaction and low effectiveness of air injection pipes, a large temperature difference was present between the entering air and combustion products.

9.3. Sensitivity analysis

In order to achieve more insight into the studied optimization problem, the sensitivity of optimum values of design parameters with changes in fuel unit cost and capital investment were investigated. Fig. 7 depicts the variation of Pareto front for different values of fuel unit cost, i.e. 0.004 $\$MJ^{-1}$ as the base value as well as 0.003 and 0.005 $\$MJ^{-1}$ respectively. Fig. 7 shows that with higher values of fuel cost, the Pareto front moves upward and to the right hand side (with higher exergy efficiencies). The upward movement of Pareto front is due to increasing the total cost as one objective function. Furthermore, it seems that the variation of objective function is less sensitive to the fuel cost in regions of higher exergy efficiency.

The variation of Pareto front with change in capital investment is also shown in Fig. 8. It is clear that with less expensive equipment the optimal system shifts to much higher efficiency to reduce fuel and environmental costs. With increase in capital investment, the optimal values of design parameters moved to the higher exergy efficiency values with the lower values of current density to maintain the fuel cost as low as possible.

The optimum values of design parameters with fuel cost and investment cost change are listed in Table 10 for a selected point

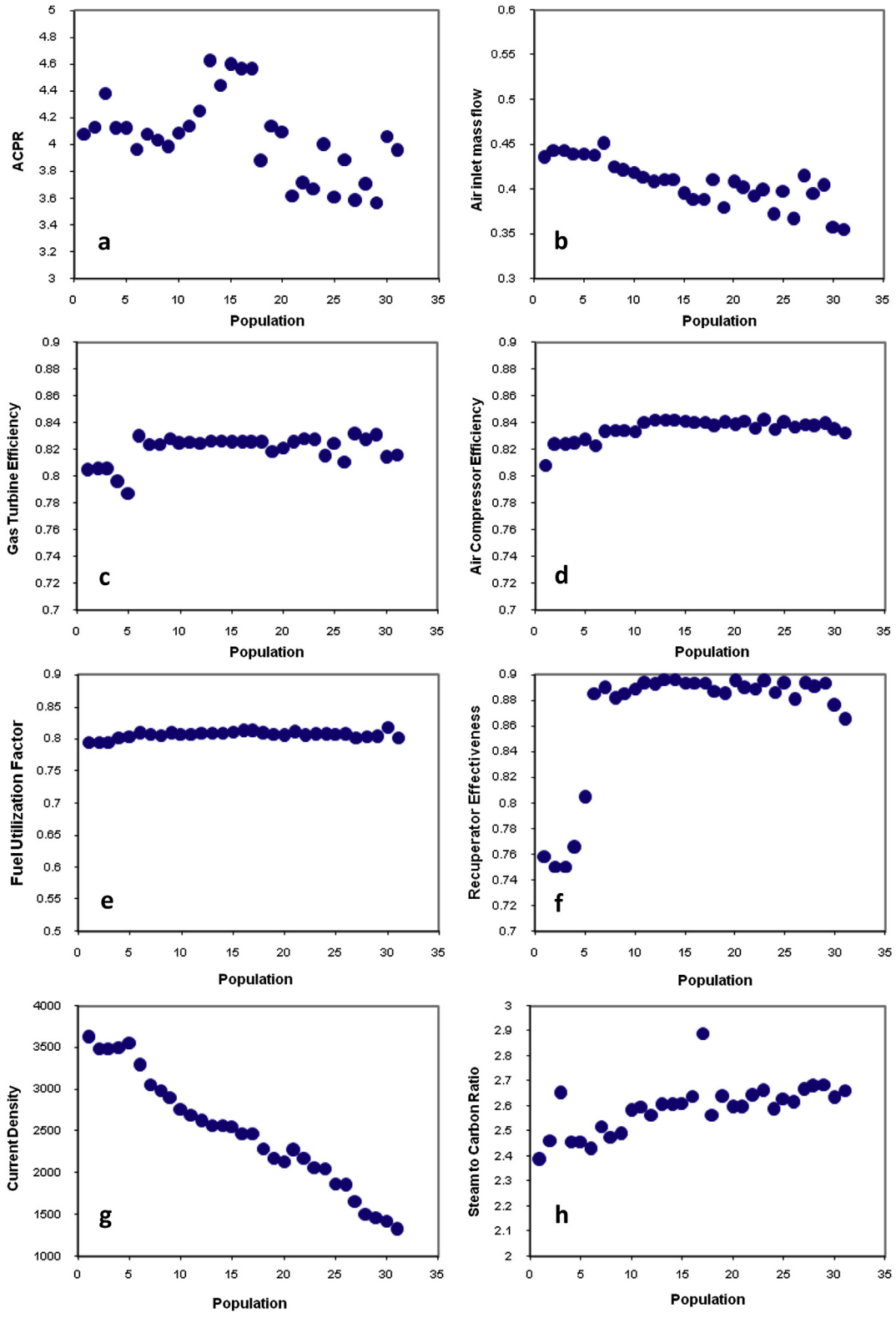

Fig. 6. Distribution of optimum values of design parameters.

Table 6
Design parameters for the optimized system selected from Pareto front.

Design parameter	Value
ACPR	4.1
η_{AC}	0.84
$m_{air,in}$ (kg s^{-1})	0.41
η_{GT}	0.82
S/C	2.6
i (Am^{-2})	2700
ε_{rec}	0.89
U_f	0.82

Table 7
Dependent system parameters the optimized system selected from Pareto front.

Dependent parameter	Value
Exergetic efficiency (%)	60.7
First law efficiency (%)	63.59
Overall CHP efficiency (%)	87.8
Total Cost rate ($\$h^{-1}$)	17.01
C_{env} ($\$h^{-1}$)	1.95
CHP Benefit ($\$h^{-1}$)	2.0
T_{cell} (K)	1253
TIT (K)	1147

Table 8
The values of temperature, pressure and mass flow rate for points in Fig. 1 for the optimized system.

Point	$\dot{m}$ (kg s^{-1})	P (bar)	T (K)
1	0.41	1	288
2	0.41	4.1	463
3	0.41	3.97	857
4A	0.0361	3.77	1253
4C	0.3821	3.77	1253
5	0.4182	3.58	1147
6	0.4182	1.1	905
7	0.3973	1.04	534
8	0.0199	1.04	637
9	0.082	1	288
10	0.082	10.9	570
11	0.082	10.57	794
12	0.3	4	288
13	0.3	4	368
14	0.4182	1.01	381

from each Pareto front. Except for the cell current density, the optimum values of other parameters did not show noticeable or meaningful variation. As explained, current density had the most prominent effect on the objective functions while the pressure ratio and inlet mass flow had lower relative change.

9.4. Change in system size (power output)

In order to study the effects of change in the system size (or the system power output) on optimum design parameters, the optimization procedure were performed for 200–1200 kW net power output. For each power output, a proper optimal point was selected and the corresponding results for relative exergy efficiency and system cost as two objective functions are shown in Fig. 9. It was noticeable that with increasing the system size, the electricity cost per kW output reduced. Another interesting point was that the optimal design parameters were very close and almost constant for different system sizes. The only varying parameters were the air compressor ratio and mass flow rate. Therefore with increase in the system size, the optimum values of fuel inlet flow as well as the size of all the system components increased which lead to a higher need for oxygen and excess cooling air in the fuel cell. Furthermore the optimum values of pressure ratio increased for a gas turbine as its flow rate increased. The change of varying optimal parameters for different sizes of hybrid SOFC–MGT system is shown in Figs. 10 and 11.

Table 9
Exergy destruction in system components for the optimized system.

Component	E_D (kW)	$E_D/E_{D,tot}$ (%)
AC	11.1	10
GT	8.74	8.2
SOFC	36.72	34
CC + AIP	44.8	42.4
REC + FPH	3.97	3.6
Rec. exchanger	2.04	1.8
Total	107.37	100

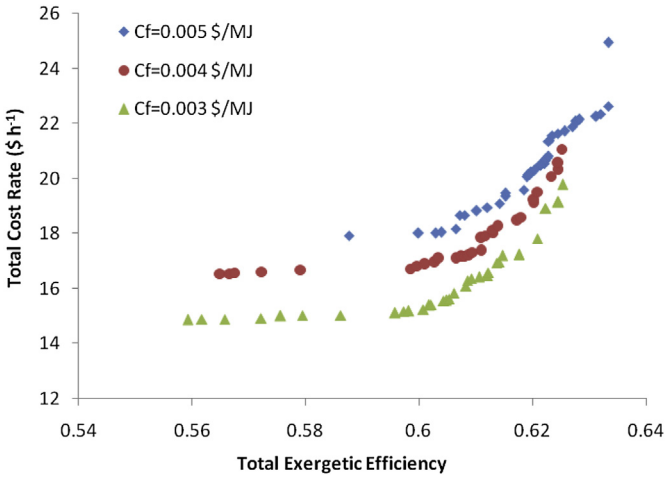

Fig. 7. The sensitivity of Pareto front shape to fuel unit cost.

10. Conclusions

A hybrid SOFC–MGT system was modeled and optimized for various power outputs (sizes) using multi-objective genetic algorithm optimization. The objective functions were selected as the total exergy efficiency and the system total cost. To consider the

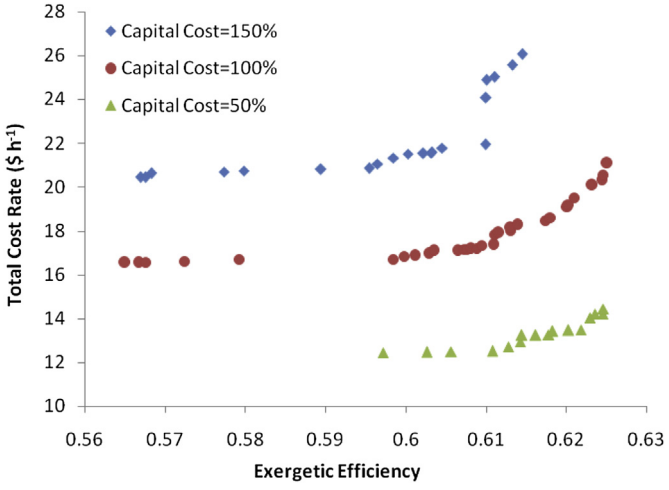

Fig. 8. The sensitivity of Pareto front shape to the capital investment cost.

Table 10
Sensitivity of the optimum values of design parameters to fuel and capital costs.

Parameter	$C_f = 0.003$	$C_f = 0.004$	$C_f = 0.005$	$C_{cap} = 50\%$	$C_{cap} = 100\%$	$C_{cap} = 150\%$
ACPR	4.2	4.1	4.3	3.97	4.1	4.21
η_{AC}	0.82	0.84	0.83	0.82	0.84	0.83
$m_{air,in}$ (kg s^{-1})	0.42	0.41	0.43	0.40	0.41	0.41
η_{GT}	0.82	0.82	0.84	0.83	0.82	0.81
U_f	0.81	0.82	0.79	0.83	0.82	0.82
ε_{rec}	0.88	0.89	0.88	0.89	0.89	0.88
i (Am^{-2})	2980	2700	2560	2445	2700	3070
S/C	2.54	2.6	2.7	2.52	2.6	2.43

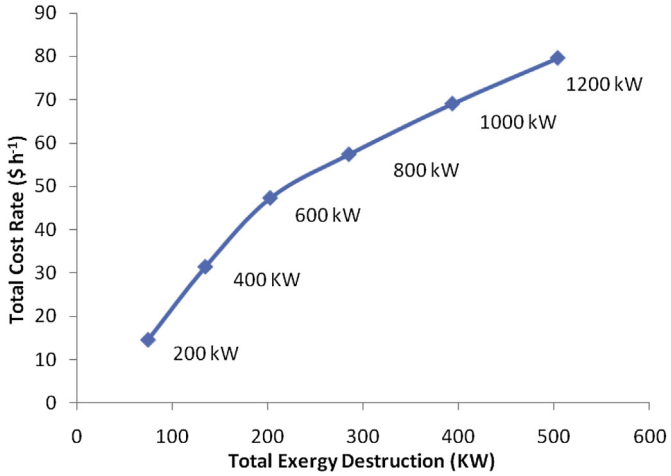

Fig. 9. Optimum values of the objective functions for various sizes of SOFC–MGT systems.

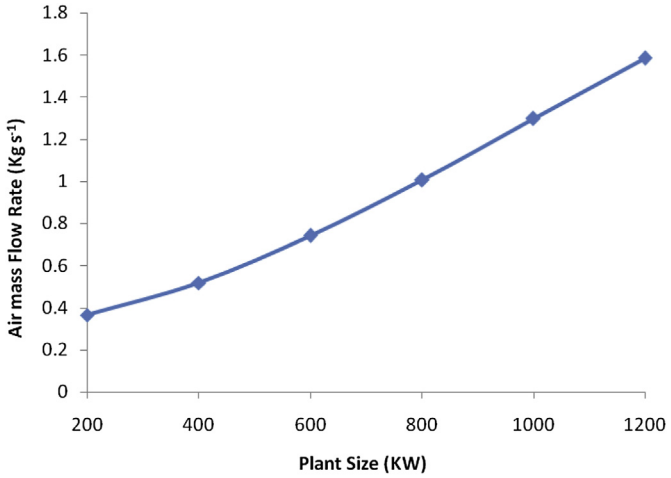

Fig. 11. The optimum values of inlet air mass flow rate for various sizes of SOFC–MGT systems.

environmental effects, a term was added to the total cost. It was observed that among design parameters of the system, the cell current density had varying nature in the allowable range of variation. This parameter played the main role in maintaining a balance between the system cost and performance. However other parameters such as the pressure ratio and air inlet flow rate had next level of changes than that for current density. The cell current density was also sensitive to the fuel unit cost and capital investment changes. Furthermore the change in system power output changed optimum values of pressure ratio and air inlet mass flow rate significantly while the optimum values of other parameters remained relatively constant with system power output.

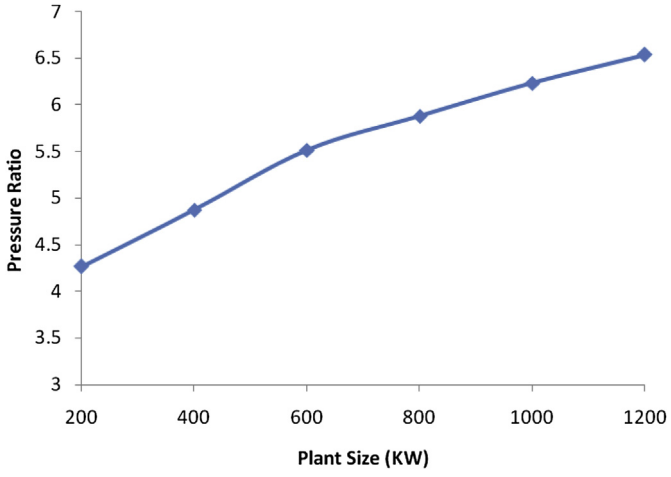

Fig. 10. The optimum values of pressure ratio for various sizes of SOFC–MGT systems.

References

[1] J. Larminie, A. Dicks, Fuel Cell Systems Explained, Wiley, New York, 2004.
[2] A.F. Massardo, C.F. McDonald, T. Korakianitis, Microturbine/Fuel-Cell Coupling For High-Efficiency Electrical Power Generation, ASME J. Eng. Gas Turbines Power 124 (2002) 110–116.
[3] A.F. Massardo, F. Lubelli, ASME J. Eng. Gas Turbines Power 122 (2000) 27–35.
[4] S. Campanari, ASME J. Eng. Gas Turbines Power 122 (2000) 239–246.
[5] P. Costamagna, L. Magistri, A.F. Massardo, J. Power Sources 96 (2001) 352–368.
[6] S.H. Chan, K.A. Khor, Z.T. Xia, J. Power Sources 93 (2001) 130–140.
[7] S.H. Chan, H.K. Ho, Y. Tian, J. Power Sources 109 (2002) 111–120.
[8] S.H. Chan, C.F. Low, O.L. Ding, J. Power Sources 103 (2002) 188–200.
[9] S.H. Chan, H.K. Ho, Y. Tian, Int. J. Hydrogen Energy 28 (2003) 889–900.
[10] S.H. Chan, H.K. Ho, Y. Tian, J. Power Sources 114 (2003) 213–227.
[11] A.F. Massardo, L. Magistri, ASME J. Eng. Gas Turbines Power 125 (2003) 67–74.
[12] P.G. Bavarsad, Int. J. Hydrogen Energy 32 (2007) 4591–4599.
[13] F. Calise, M. Denticed'Accadia, A. Palombo, L. Vanoli, Energy 31 (2006) 3278–3299.
[14] F. Calise, A. Palombo, L. Vanoli, J. Power Sources 156 (2006) 225–244.
[15] F. Calise, M. Denticed'Accadia, A. Palombo, L. Vanoli, M.R. von Spakovsky, J. Power Sources 159 (2006) 1169–1185.
[16] F. Calise, M. Denticed'Accadia, A. Palombo, L. Vanoli, M.R. von Spakovsky, Energy 32 (2007) 446–458.
[17] N. Autissier, F. Palazzi, F. Marechal, J. Van Herle, D. Favrat, ASME J. Fuel Cell Sci. Technol. 4 (2007) 123–129.
[18] L. Duan, B. He, Y. Yang, Int. J. Energy Res. 35 (2011) 721–732.
[19] J.P. Holman, Heat Transfer, ninth ed., McGraw-Hill, New York, 2001.
[20] S. Sanaye, H. Hajabdollahi, Appl. Energy 87 (2010) 1893–1902.
[21] S. Sanaye, H. Hajabdollahi, Appl. Therm. Eng. 30 (2010) 1937–1945.
[22] W.M. Kays, A.L. London, Compact Heat Exchangers, third ed., McGrawHill, New York, 1984.
[23] S. Kakac, H. Liu, Heat Exchangers, Selection Rating and Thermal Design, second ed., CRC Press, 2002.
[24] E.M. Smith, Advances in Thermal Design of Heat Exchangers, John Wiley and Sons, Ltd, 2005.

[25] S. Sanaye, M. Ziabasharhagh, M. Ghazinejad, Int. J. Energy Res. 33 (2009) 766–777.
[26] S. Sanaye, M. Raessi Ardali, Appl. Energy 86 (2009) 895–903.
[27] A. Bejan, G. Tsatsaronis, M. Moran, Thermal Design and Optimization, John Wiley and Sons, New York, 1996.
[28] Siemens-Westinghouse Power Corporation, Pressurized Solid Oxide Fuel Cell/Gas Turbine Power System. Final Report, for US Department of Energy, February 2000.
[29] A. Lazzaretto, A. Toffolo, Energy 29 (2004) 1139–1157.
[30] A. Boudghene Stambouli, E. Traversa, Renewable Sustainable Energy Rev. 6 (2002) 433–455.
[31] R.J. Braun, Optimal Design and Operation of Solid Oxide Fuel Cell Systems for Small-scale Stationary Applications. Doctoral Thesis, University of Wisconsin–Madison, 2002.
[32] P.L. Yu, Multiple-criteria Decision Making, Concepts, Techniques, and Extensions, Plenum Press, New York, 1985.
[33] D.L. Olson, Decision Aids for Selection Problems, Springer, New York, 1996.